AMS Home   Journals Home   Journal Archive   Subscribe   For Authors   Help   Advanced Search   [Search] Go

Full Text View

Slope-Enhanced Fission of Salty Hetons under Sea Ice

Shenn-Yu Chao

Horn Point Laboratory, University of Maryland Center for Environmental Science, Cambridge, Maryland

Ping-Tung Shaw

Department of Marine, Earth and Atmospheric Sciences, North Carolina State University, Raleigh, North Carolina

ABSTRACT

Ocean responses to a single brine source under ice and over a sloping bottom are investigated in numerical experiments. Brine sources considered herein are often much stronger than that anticipated from a single seawater freezing event in a time span of about 10 days. The authors have no evidence that such strong sources exist in the ocean, but the consequent heton-like eddies manifest interesting features over a bottom slope. The numerical model contains a stratified ocean capped by an ice layer. The convection initially generates a top cyclone and a submerged anticyclone vertically stacked together. Under sea ice, the top cyclone dissipates in time and often breaks up into several distinct cyclonic vortices. Through heton-type couplings, the breakaway shallow cyclones are often able to tear the underlying anticyclone apart to form distinct anticyclones. Top cyclones are eventually annihilated by ice-exerted friction, leaving submerged anticyclones in stable existence. Fission from a pair of vertically stacked baroclinic vortices is a fundamental process associated with a strong brine source under sea ice. A bottom slope generally enhances fission, often increasing the number of subsurface anticyclones or causing the resulting anticyclones to break farther away from the source. The slope enhancement is consistent with the potential vorticity conservation requirement and a changing Rossby radius with water depths. The foregoing conclusions remain the same in cases with a stationary brine source moving rigidly with a uniform current. Under the less likely scenario of a stationary source embedded in a mean flow, brine waters spread downstream and become less effective in producing distinct vortices. Granting the occurrence of strong baroclinic vortices under sea ice, the preferable increase of anticyclones at depths may help explain the overwhelming predominance of submerged anticyclones in the ice-covered Arctic Ocean.

Options:
- Create Reference
- Email this Article
- Add to MyArchive
- Search AMS Glossary

Search CrossRef for:
- Articles Citing This Article

Search Google Scholar for:
- Shenn-Yu Chao
- Ping-Tung Shaw

1. Introduction

Under Arctic sea ice, the shallow halocline in the top 400 m of the Beaufort Sea harbors a field of predominantly anticyclones ([Manley and Hunkins 1985](#)). These eddies are generally small, having radii ranging from 5 to 30 km and rotation speeds up to 60 cm s^{-1}. They normally exist in a depth range between 50 and 300 m beneath the sea surface. The effect of planetary dispersion is expected to be insignificant for these small eddies and should not be used as an argument in favor of anticyclones.

In the baroclinic regime, fission of a vertically stacked pair of opposite eddies had been demonstrated before. A cylinder of positive density anomaly would generate a top cyclone and a bottom anticyclone. The pair could disintegrate into a number of baroclinic eddies in a rotating tank setting ([Saunders 1973](#)). The resulting number of eddies increases with the strength or radius of the initial density anomaly. A pair of baroclinic eddies similar to those produced in a rotating tank by Saunders was later coined the term "cold heton" by [Hogg and Stommel (1985)](#). Since salinity is the major indicator of density variations in the Arctic, a cold heton at midlatitudes would correspond to a salty heton in the Arctic. The feasibility of fission from a pair of baroclinic eddies was subsequently checked against a few fundamental integral constraints by [Nof (1991)](#). A few assumptions on the strength and structure of the initial pair and resulting pairs were made by Nof to render the problem analytically tractable. Fission was found to be possible if certain criteria are met. In spite of the efforts by [Saunders (1973)](#) and [Nof (1991)](#), mechanisms leading to fission remain to be elucidated.

[Chao and Shaw (1996)](#) investigated how a shallow brine source generates a subsurface anticyclone under sea ice. The ice layer was assumed to be highly compacted and therefore treated as a no-slip surface. [Figure 1](#) illustrates the outcome. Under sea ice, a pulse of shallow brine forcing is applied for a finite time. The radius of salinity forcing is less than the first baroclinic Rossby radius. A pair of eddies is produced and has radii comparable to one Rossby radius. The top cyclone dissipates in time by the ice-exerted friction, leaving the subsurface anticyclone in sole existence. Isohalines are displaced away from a central surface in the submerged anticyclone. A subsurface anticyclone thus produced contains essential observed features. Eddies of this type appear to be quite stable when in sole existence. A vertically sheared current was later imposed to move the eddies ([Chao and Shaw 1998](#)). Given modest vertical shear, most of these eddies manage to survive while in translation.

The treatment of an ice layer as a no-slip surface is stabilizing. The vertical shear associated with the circulation of the top cyclone and the subsurface anticyclone is quickly reduced as the top cyclone is annihilated by ice-exerted friction, rendering a submerged anticyclone baroclinically stable. If a mobile ice layer is used, the top cyclone is able to survive longer and the pair is subject to baroclinic instability for a longer period of time. In this case, the top cyclone often breaks up into several smaller cyclones during the spinup period, and fission of the lower anticyclone is likely. Three possible scenarios in the case of two breakaway cyclones in a deep basin are illustrated in [Fig. 2](#). If the baroclinic instability is weak ([Fig. 2a](#)), the cyclones (unshaded) do not break too far away from the initial center of their parent cyclone, and thereafter corotate anticyclonically about the subsurface anticyclone (shaded). In this case, coupling is between each satellite cyclone and the submerged anticyclone, and the anticyclone remains intact. This type of heton coupling is akin to that originally envisioned by [Hogg and Stommel (1985)](#). For stronger instability ([Fig. 2b](#)), satellite cyclones are not trapped in an orbit about the submerged anticyclone but break away radially. Through heton-type coupling, each breakaway cyclone copropagates away with a small portion of the submerged anticyclone below. In this case fission is still weak in the anticyclone. If the initial instability of the top cyclone is very strong ([Fig. 2c](#)), the submerged anticyclone can be torn apart by breakaway cyclones, leaving little anticyclonic vorticity in the parent pool. In all cases, satellite cyclones are dampened by ice-exerted friction in time, leaving submerged anticyclones in stable existence thereafter.

A vertically stacked pair of a top cyclone and a subsurface anticyclone possess little relative vorticity when averaged vertically. Under this circumstance, a bottom slope should have little effect on the baroclinic pair. This is not the case after the breakup of the top cyclone;relative vorticity is negative for the anticyclone and positive for cyclones when averaged vertically. Changing Rossby radii may also modify the behavior of eddies as they enter waters of different depths. Thus, the fission process described in [Fig. 2](#) may be modulated by a bottom slope. Our previous studies on this subject dealt with brine and freshening sources over a deep and flat basin. The Rossby radius was larger than the forcing radius, and topographic variations were excluded. In this limit fission is weak, and a mobile ice layer was often needed to activate fission. Dominance of submerged anticyclones over subsurface cyclones under a mobile ice layer has been demonstrated by arranging brine and freshening sources in pairs ([Chao and Shaw 1999a](#)) and in rows ([Chao and Shaw 1999b](#)). This paper presents a departure from our previous studies by examining fission of hetons under a single brine source over a bottom slope with and without a mean flow, using a model of a stratified ocean with an ice layer. The survivability of brine-induced anticyclones is investigated.

For lack of better horizontal resolution and nonhydrostatic processes, the present model is ill-suited to simulate the initial phase of shallow convection in the Arctic Ocean. This is apparent from the numerical simulations of [Smith and Morison](#)

(1993) and Kämpf and Backhaus (1998). Imagine a fluctuating wind carrying cold and dry Arctic air over a patchy ice layer. Intermittent oceanic heat losses freeze seawater and release brine in leads and polynyas. The shallow convection is initially characterized by fine-scale sinking plumes of a few hundred meters in horizontal dimensions (Carsey and Roach 1994), coalescing in time. Cascading toward large scales (Smith and Morison 1993; Kämpf and Backhaus 1998) must be halted at scales around a Rossby radius. The initial cascading from small scales to a Rossby radius is beyond the scope of this work. Rather, our experiments begin with a brine source having a radius somewhat less than a Rossby radius. The brine source is maintained for finite duration because subsequent redistribution of the patchy ice layer may shield the source region from further cooling-induced brine convection. Cooling over a longer period of time may result in downslope bottom density plumes along the sloping bottom. This process is circumvented by cutting off the source after finite duration, and by the presence of a halocline, which inhibits unrestricted sinking motion.

To investigate fission, brine sources used in the present hydrostatic model are generally much stronger than that produced by a single seawater freezing event in a time span of about 10 days. The purpose is to generate strong baroclinic vortices independent of the means. Weaker sources can also lead to fission if the upper ocean pycnocline is very weak; this limit is discussed in appendix A as a reality check. There is no evidence to suggest such strong sources exist in nature. Perhaps strong baroclinic vortices can be produced by horizontal processes rather than vertical convection. Perhaps a strong salinity anomaly may result from a series of freezing events or by merging with adjacent sources, possibly with the help of local flow convergence. In any case, interesting consequences follow after strong baroclinic vortices are produced by strong brine sources. In this light, the numerical experiments begin with a strong brine source capped by a motionless or a uniformly moving ice layer.

2. Model description

On an f plane with $f = 1.4 \times 10^{-4}$ s^{-1}, a dynamic sea ice model using the viscous plastic rheology of Hibler (1979) is coupled to a primitive-equation ocean model to facilitate the study. Forcing at air–ice interface and thermodynamic coupling at ice–water interface are excluded for simplicity. Under a finite-difference approximation, governing equations for the ice layer are solved for horizontal velocities (u and v), ice concentration (A), and ice thickness (h) averaged over each mesh. The initial ice layer is either motionless or moving with a uniform ocean current, having a uniform concentration of 0.7 and a uniform thickness of 2 m. Subsequent ice fluctuations and variations in A and h are entirely driven by a brine source below. In this application the ice cover essentially serves as a viscous layer dampening ocean surface currents. The viscous-plastic rheology is extensively documented in literature. For these reasons, details about the ice layer formulation are placed in the appendix B.

Under the ice layer, a cross-isobath vertical section of the ocean basin is illustrated in Fig. 3 . The square basin has a length scale of 120 km with a horizontal resolution of 2 km. A right-handed Cartesian coordinate system is placed on the ocean surface at the center of the basin. The bottom depth is uniform in the x direction. In the cross-isobath (y) direction, bottom depth either increases in a piecewise linear fashion from h_1 to h_2 or is constant with $h_0 = (h_1 + h_2)/2$ (Table 1). The typical choice of a bottom slope is from 200 to 500 m over a distance of 80 km. Steeper slopes do exist in the Arctic Ocean. We have refrained from approaching the steep-slope limit to avoid the buildup of truncation errors in this σ-coordinate model. The vertical resolution is refined near the surface in a σ-coordinate formulation. There are 28 layers in the vertical. The deepest layer is 0.1055 of the local water depth. The thickness of each layer above is 0.9 of that immediately below. The top layer is 0.0061 of the local water depth. The ocean is initially motionless or moving uniformly along isobaths, and contains a typically observed halocline of the Arctic Ocean (Fig. 3). The salinity S in practical salinity units is $35 - \Delta S$ in the top 50 m of the water column and increases downward to 35 according to $S(z) = (35 - \Delta S) - \Delta S \tanh[(z - z_0)/D]$, where $z_0 = -50$ m, $D = 450$ m, and ΔS characterizes the strength of halocline in the upper ocean. In most cases, ΔS is set to 4.5 psu to produce a strong halocline typically observed in the Beaufort Sea (Manley and Hunkins 1985). Ocean temperature is fixed at 2°C throughout the numerical simulation. The choice of a temperature is not important in this model. What really counts is the dependence of seawater density on salinity. Whether the temperature is 2°C or at the freezing point, this dependence varies little. Figure 4 shows the first two baroclinic Rossby radii associated with the ocean stratification as functions of local bottom depth. The first Rossby radius is more relevant since eddies tend to adjust to the largest radius.

The numerical ocean model is hydrostatic and Boussinesq, following that of Blumberg and Mellor (1987). Vertical mixing coefficients are determined by a level-2.5 turbulence closure scheme (Mellor and Yamada 1974). In this closure scheme, the unstable stratification is gradually removed by enhancing diffusivity instead of instantaneous convective adjustment. Leaving turbulence quantities aside, the model computes three-dimensional velocities (U, V, W), salinity (S) and sea level at fixed time intervals. The momentum and continuity equations are conventional with no external forcing. Forcing is in the salinity equation,

$$\frac{DS}{Dt} = F(x, y, z, t) + \nabla \cdot (A_H \nabla S) + \frac{\partial}{\partial z}\left(\kappa \frac{\partial S}{\partial z}\right),$$

where $D/Dt = \partial/\partial t + U\partial/\partial x + V\partial/\partial y + W\partial/\partial z$, ∇ is the horizontal gradient operator, A_H and κ are the horizontal and vertical mixing coefficients, respectively. The shallow salinity source F is given by

$$F = F_0 \exp[-(r/r_0)^2] \exp[-(z/z_1)^6]H(T - t),$$

where F_0 is the source strength in units of psu day^{-1}, and r_0 (=6 km) and z_1 (=50 m) characterize the e-folding radius and depth, respectively. The radial distance (r) is measured from the center of the brine source. Typically, the brine source is assumed to be over water depths ranging from 350 to 500 m in this model. Otherwise, a bottom slope in much deeper waters would have little effect on salty hetons aloft. Referring to Fig. 4 ⊙▬, the e-folding forcing radius (r_0) is less than the first baroclinic Rossby radius in water depths more than 350 m or so. With a typical T of several days, the Heaviside step function (H) turns off the salinity forcing after $t = T$. The initial ocean is either motionless or moving with a uniform speed $U_0 = 5$ cm s^{-1}. The uniform current is along-isobath, moving with shallower waters on either left or right of the current.

The ice layer and the ocean are cyclical in the x direction. Zonal boundaries at $y = \pm60$ km are open; all ice and ocean variables have zero normal gradients on these two boundaries. The shear stress at the ice-ocean interface is quadratic, given by

$$\tau = \rho_i C_i |U - u|(U - u),$$

where $\rho_i = 0.91$ gm cm^{-3} is the ice density, $C_i = 0.02$ is the drag coefficient, and U and u are ocean and ice velocity vectors, respectively. The drag coefficient (C_i) is comparable to measured values at an ice–sea interface (Pease et al. 1983). A quadratic stress is also enforced at the ocean bottom with a dimensionless drag coefficient of 0.0025.

By setting up the model this way, the ocean is initially driven by a shallow salinity source near the surface. Surface ocean currents, in turn, induce ice motions. Being highly viscous, the ice layer decelerates quickly and thereafter dissipates surface ocean currents. Top eddies lose strength in time, and are eventually annihilated by friction exerted by sea ice. Some specifics about the ocean model were given earlier in Chao and Shaw (1996) and will not be repeated below.

Over a sloping bottom, calculations of cross-isobath baroclinic pressure gradients in a σ-coordinate ocean model contain truncation errors (Haney 1991). In the present model the ambient hydrostatic pressure specified in the initial condition is removed before baroclinic pressure gradients are computed. This measure eliminates most truncation errors. To verify, the coupled model has been run in the absence of brine forcing. Relative to the motionless state, the truncation error over a typical bottom slope employed in this study manifests weak along-isobath currents. The currents as a measure of truncation errors accumulate to less than 0.5 cm s^{-1} over a simulation period of 15 days. This error is at least one order of magnitude smaller than the dominant speeds of interest.

3. Numerical results

Table 1 ⊙▬ lists all numerical experiments discussed in this paper. Each experiment over a sloping bottom (denoted by "S") is accompanied by a flat bottom experiment using the average depth of the basin (denoted by "F"). Experiments 1S and 1F use a short but very strong pulse of brine forcing ($F_0 = 1.05$ psu day^{-1}, $T = 5$ days). The water depth increases from 200 to 500 m in experiment 1S and is uniform at 350 m in experiment 1F. Using the same basins, the brine source in experiments 2S and 2F are weakened twofold ($F_0 = 0.5$ psu day^{-1}) but maintained twice as long ($T = 10$ days).

Experiments (3S, 3F) differ from (2S, 2F) by further reducing the brine strength twofold to 0.25 psu day^{-1}. Experiments (4S, 4F) further reduce the brine source strength twofold to 0.125 psu day^{-1}, but the upper ocean halocline (characterized by ΔS) is reduced ninefold. This is the limit in which a reasonably weak brine source can produce subsurface anticyclones and fission. Experiments (1S, 1F) are further generalized by including an eastward mean flow (denoted by "E") and a westward mean flow (denoted by "W") over the sloping bottom, and only an eastward flow over the flat basin. Similar extensions have also been made for experiments (3S, 3F).

Relating our brine strength to reality, it is noted that new ice formation rates in coastal polynyas range up to 0.3 m per day in the Arctic (Smith et al. 1990). The salinity production rates in our model, when averaged over a cylindrical source volume of 50 m in height and 12 km in diameter, are 0.59, 0.29, 0.15, and 0.075 psu per day for the first, second, third, and fourth series of experiments. These rates would correspond to ice formation rates of (0.8, 0.4, 0.2, 0.1 m) per day if all salt is released during the 5- or 10-day freezing period. These rates are high especially for the first two series of experiments, noting that not all salt is released during initial freezing. Alternatively, one could spread the salinity forcing over a longer

period to decrease the rates;conclusions would be similar to those to be established below. Higher rates are chosen mainly for two reasons. First, there is a real geophysical interest in the stability of heton-like vortices over a bottom slope, independent of how these vortices are generated. In this light the strong source scenario can be regarded as experiments examining the effect of suddenly imposed ice layer on existing hetons. Second, the grid-scale damping in this coarse grid model is believed to be much larger than in a real ocean. Forcing enhancement helps overcome the numerical damping. Taking these concerns into consideration, brine sources in the first, second, and third series of experiments are considered to be superstrong, strong, and moderate, respectively, from our perspective.

a. A superstrong source

In this case the brine release rate is considerably higher than what a realistic freezing event can provide in polar oceans. Figure 5 ⊙▬ shows ice drift velocities and ice concentrations at days 5 and 15 in the sloping bottom experiment 1S. The salinity forcing is maintained for the first 5 days. Thereafter the ice layer is driven by decaying ocean surface currents. Brine convection forces the ice layer to diverge continuously. Conceivably, the ice layer divergence enhances oceanic cooling and brine convection if the atmospheric cooling effect is included in the model. This positive feedback mechanism is excluded herein. Cyclonic motions prevail inside the shaded low concentration patch, indicative of ocean surface currents below. In time, viscous dissipation smears out cyclonic vorticities and diminishes ice drifts. Driven by the same divergence of ice motions, variations in ice thickness are similar to that in ice concentration and therefore not shown. A thinner ice layer would coexist with a lower ice concentration. With respect to ocean responses, the ice layer response is relatively featureless and therefore will not be further illustrated.

Features at 30-m depth in the ocean (Fig. 6 ⊙▬) resemble that of the ice layer to a degree. The shaded high saline patch at day 5 is characterized by a cyclonic circulation and disturbances around the rim. By day 15, the cyclone breaks into two: one to the northeast and the other to the southwest. Looking radially outward from the initial brine center, the two cyclones appear to the left of high salinity anomalies associated with the submerged anticyclones at greater depths. This is the heton-type coupling to be commented on later. A minor patch of high salinity with weak anticyclonic rotation is ejected to the east. Anticyclonic vorticity is also evident at the location of the brine source. Currents at 30 m depth decay in time as a result of ice-exerted friction.

Downward in the water column, salinity surpluses become salinity deficits for subsurface anticyclones. Corresponding flow and salinity fields at 180 m (Fig. 7 ⊙▬) illustrate fission of the submerged anticyclone. The anticyclone at day 5 becomes four at day 15. Sequential snapshots at shorter time intervals (not shown) reveal that only the three stronger anticyclones aligned in the northeast–southwest direction originate from the parent anticyclone. The weaker one to the east is newly produced by the ejected saline parcel aloft (see Fig. 6 ⊙▬, bottom panel). There is also a weak cyclone to the east of the southernmost anticyclone. Since there is no freshening source aloft, the weak cyclone is driven by the shear between anticyclones.

Evidence of copropagating pairs of top cyclones and subsurface anticyclones can be better illustrated by the vertically integrated stream function. Figure 8 ⊙▬ shows stream functions at days 5, 10, and 15. At day 5, the top cyclone and subsurface anticyclone essentially overlap, producing little vorticity when integrated vertically. Two weak cyclonic vortices (C1 and C2) appear to the northwest and southeast of the brine source. The two cyclones rotate anticyclonically about the anticyclone while breaking away. By day 10, the heton-type coupling as indicated by H1 and H2 becomes evident. Cyclone C1 pulls the subsurface anticyclone (shaded) to the northeast, while cyclone C2 tends to copropagate with the submerged anticyclone to the southwest. The strain produces two new submerged anticyclones at day 15, leaving the remains of the parent anticyclone in between. As cyclones continue to diminish after day 15, the heton-type coupling becomes exceedingly weak, leaving all subsurface anticyclones in stable existence. The H1 pair moves farther to the northeast than H2 to the southwest from the origin. The greater distance into deeper waters is caused by the dominance of cyclone C1 over C2. Cyclone C1 intensifies as it enters deeper waters, carrying anticyclonic vorticity below with it.

In experiment 1F, a flat bottom is placed at the mean basin depth (350 m). Flow and salinity features at day 15 are shown in Fig. 9 ⊙▬ at 30-m and 180-m depths. Two breakaway cyclones are present at 30 m at day 15. Following the breakup of the top cyclone, the subsurface anticyclone at 180-m depth also splits into two. An additional submerged anticyclone to the west is much weaker. Heton-type coupling is evident. Radially outward from the initial brine center, a submerged anticyclone appears on the right of a propagating pair. Figure 10 ⊙▬ shows vertically integrated stream functions for the flat-bottom experiment at days 5, 10, and 15. Shaded and unshaded vortices indicate anticyclones and cyclones, respectively. By day 10, the breakaway cyclone C1 carries a portion of the submerged anticyclone northeastward to form a propagating heton (H1), while cyclone C2 copropagates southward with the remaining anticyclone as another heton (H2). By day 15, the strain produces two distinct anticyclones, leaving little anticyclonic vorticity in between. Top cyclones decay continuously in time. Both hetons propagate along curved paths in favor of the dominant partners. For heton H1, the subsurface anticyclone dominates and therefore stays in the inner orbit of a curved path. For H2, the top cyclone (C2) dominates and forces the anticyclone to orbit around it.

Instabilities in Experiments 1S and 1F are strong, corresponding to the scenario shown in Fig. 2c ⊙. Ignoring the weak ones, three anticyclones are produced in Fig. 7 ⊙, while two appear in Fig. 9 ⊙. In this sense, fission is enhanced by the presence of a slopping bottom.

b. Strong and moderate sources

The resulting anticyclones at day 15 in experiments 2S and 2F, where the pulse of salinity forcing is spread out to 10 days, are shown in Fig. 11 ⊙. At 180-m depth, fission produces three anticyclones over the bottom slope but essentially two anticyclones in the flat-bottomed case. In both cases, fission is driven by two major breakaway cyclones aloft similar to that in experiments 1S and 1F. Over the sloping bottom, vortices after fission tend to align in the cross-isobath directions, and the parent anticyclone moves somewhat to deeper waters after fission. Over the flat bottom, vortices after fission need not be aligned in the north-south directions, and the parent anticyclone stays more or less in the original position after fission. Leaving minor variations aside, the strength of fission corresponds to a scenario depicted in Fig. 2b ⊙.

Weakening the forcing further, the fission process becomes exceedingly slow and it takes longer simulation time to see the difference induced by a bottom slope. Anticyclones at 180 m depth are shown in Fig. 12 ⊙ at day 25 in experiments 3S (upper panel) and 3F (lower panel). If a bottom slope is imposed, two patches of salinity anomalies varying in size spin off to the north. The parent anticyclone to the south is also elongated. Without a bottom slope, locations of the two spinoff anticyclones are essentially symmetrical about the original brine center, leaving little vorticity in the parent pool. The slope-enhanced fission is becoming much less visible. Thus, in a strong halocline typically observed in the Beaufort Sea, the slope-enhanced fission cannot be produced by a single cooling event in a time span of about 10 days. Reinforcement of the source strength through stochastic means may be necessary to produce the slope-enhanced fission. Alternatively, fission and its enhancement by a bottom slope can be produced by a very weak brine source if the halocline is exceedingly weak. This will be discussed in appendix A. The result from experiment 3F (Fig. 12 ⊙, lower panel) gives a distinct impression that fission somehow becomes stronger for a weaker source, resembling that as depicted in Fig. 2c ⊙. It should be reemphasized that the two breakaway anticyclones in experiment 3F take 25 days to develop. Comparing to a stronger source in experiment 2F (Fig. 11 ⊙, lower panel), it is clear that the seemingly strong fission under the weak source in experiment 3F is slow because it takes 10 more days to develop.

c. Effect of mean flow

Mean flow may be imposed in two ways. A more realistic scenario is to allow the brine source to move uniformly with the mean flow. In this limit the foregoing results remain valid under a coordinate transformation to the moving frame. The other scenario of a stationary source embedded in a uniform flow is less realizable in nature but still of geophysical interests, and will be examined below. The likelihood of this scenario increases if the source drifts at a speed somewhat different from the ambient flow. In this case the imposed mean flow can be considered as the speed difference between the source and the actual mean flow.

For an eastward flow and a superstrong source over the sloping bottom (experiment 1SE), Figure 13 ⊙ shows the flow and salinity fields at 180-m depth at days 5, 10, and 15 (left panels). To better illustrate heton-type couplings, corresponding stream function anomalies after removing the zonal average are shown in right panels. Bars on top and right of each panel indicate the stationary brine location. The mean flow spreads saline waters continuously downstream and therefore weakens fission. Nevertheless, three distinct anticyclones are formed instead of a continuous streak. Arrows in the middle right panel indicate copropagation directions due to heton-type couplings between top cyclones and subsurface anticyclones. In addition to streamwise advection, trajectories of subsurface anticyclones are also affected by heton-type propagation. Anticyclone A in the bottom left panel becomes stronger as it enters deeper waters.

Figure 14 ⊙, from experiment 1SW, illustrates a similar advection by a westward flow. As before, three distinct anticyclones are formed and downstream advection is modified by the self-propagating tendency of hetons. Anticyclone B in the bottom left panel gains strength and size as it enters deeper waters. If top cyclones are absent, a subsurface anticyclone in sole existence normally moves to the left of a mean flow (Chao and Shaw 1998). Such movements are mostly offset by hetonlike couplings. In this complex setting, lateral eddy movements can result from current-eddy interactions, topographic effects and hetonlike couplings. With a strong source and a weak mean flow, Figs. 13 ⊙ and 14 ⊙ suggest that hetonlike couplings dominate.

Fission in a mean flow weakens if the bottom slope is removed. Figure 15 ⊙, from experiment 1FE, illustrates that the spinoff anticyclones are much weaker than their counterparts over a sloping bottom. The strength of breakaway anticyclones can be measured by the number of contours within each vortex. Comparing Fig. 13 ⊙ and Fig. 15 ⊙, spinoff anticyclones are considerably weaker over the flat bottom. A large portion of anticyclonic vorticity remains in the parent pool (C in bottom right panel). As in the last two figures, heton-type couplings modulate the downstream movement. With or without a mean flow, the enhancement of fission by a bottom slope is evident for a superstrong brine source.

If a weaker source is used, such as in the third series of experiments, a streak of saline waters will form downstream of the source, unable to produce distinct anticyclones or fission. Results from experiments (3SE, 3SW, 3FE) are otherwise unremarkable and therefore not shown.

4. Discussion and conclusions

At scales comparable to a baroclinic Rossby radius, fission is seen as a fundamental process for a pair of strong baroclinic eddies under sea ice. In a timescale of about 10 days, a very strong brine source is needed to produce strong baroclinic vortices and fission in a strong halocline typically observed in the Beaufort Sea. If the halocline weakens considerably, the brine source strength can be reduced to observed rates to produce subsurface anticyclones and fission, but the resulting rotation speeds are quite weak (see Appendix A). When fission occurs, the top cyclone first breaks up into a few cyclonic vortices. Through the heton-type coupling, the spinoff cyclones are capable of tearing the underlying anticyclone apart into a few distinct vortices. The resulting number of subsurface anticyclones varies, depending on how volatile the initial breakup of the top cyclone is. It is also clear that a bottom slope often enhances fission. What is the role of the ice layer in modulating fission? Would fission be similarly active if a freshening source rather than a brine source is used? Our findings cannot be put in proper perspectives before these questions are answered.

An ice layer is essential for the increase of subsurface anticyclones. Without ice-exerted friction, the top cyclone generated by a brine source would be much stronger than the anticyclone below. The subsequent breakup of the top cyclone would be too volatile to produce distinct subsurface anticyclones. Instead, the parent anticyclone is often torn apart as thin filaments. The ice layer brings down the rotation speed and slows down the breakup of the top cyclone. The gentler breakup aloft allows the subsurface anticyclone to disintegrate slowly, producing distinct anticyclones. At the other extreme, fission may be annihilated if the ice layer is treated as a no-slip surface especially when the forcing radius is considerably smaller than a Rossby radius. In this limit the top cyclone is often quickly dissipated by friction before carrying a portion of the submerged anticyclone away to produce fission. This is the limit explored by Chao and Shaw (1996, 1998).

Regardless of how much surface friction is exerted, fission from a pair of baroclinic eddies produced by a freshening source is consistently much weaker than that generated by a comparable brine source. In the limit of no surface friction, the breakup of top anticyclone produced by a freshening source is much slower than that of a top cyclone generated by a comparable brine source. The gentler breakup often produces a few distinct cyclones below through the heton-type coupling. In a similar setting, a submerged anticyclone induced by a comparable brine source would have been torn apart as thin filaments. If an ice layer is superimposed, the breakup of a top anticyclone produced by freshening becomes exceedingly weak, and is in most instances unable to increase the number of submerged cyclones below.

The preferable increase of subsurface anticyclones under sea ice is ultimately related to the baroclinic instability that fuels the fission. Under a freshening source, the spin up of a pair of baroclinic vortices is essentially a geostrophic adjustment process which releases a modest amount of potential energy for consumption (Rossby 1938). Under a brine source, however, downward convection soon takes over after a brief geostrophic adjustment period, releasing even more potential energy to produce eddies. This point was elaborated in Chao and Shaw (1996). With or without fission, subsurface anticyclones induced by brine sources are therefore consistently stronger than submerged cyclones produced by freshening sources. This conclusion holds not only for a single source but also in a group setting. When equal numbers of comparable brine and freshening sources are used, the winning vortices at depths are consistently anticyclonic in terms of both numbers and strength. This is true whether brine and freshening sources are lined up in pairs (Chao and Shaw 1999a) or in rows (Chao and Shaw 1999b).

Enhancement of fission over a sloping bottom is consistent with potential vorticity constraints. Figure 16 ⚙ illustrates schematically how a sloping bottom enhances fission of a submerged anticyclone produced by a brine source. Under a brine source, the shallow cyclone and the anticyclone below initially overlap, producing little relative vorticity when integrated vertically. A subsequent breakup of the top cyclone into two vortices C1 and C2, for example, generates net anticyclonic vorticity in the parent pool and cyclonic vorticities in the breakaway cyclones when integrated vertically (Fig. 16a ⚙). The two spinoff cyclones rotate about the submerged anticyclone in a clockwise sense. The corotation is manifested by heton-type couplings as indicated by H1 and H2. Cyclone C1 would intensify as it enters deeper waters to conserve potential vorticity. Cyclone C2 would decay somewhat when entering shallower waters. In addition to potential vorticity constraints, a changing Rossby radius with water depths may have also contributed to the asymmetry between two shallow cyclones. Cyclone C1 enters waters with a larger Rossby radius, and therefore should intensify and expand at the expense of potential energy. Cyclone C2 cannot shrink as it enters waters with a smaller Rossby radius, as a reverse geostrophic adjustment is prohibited. Thus, heton coupling H1 should be stronger than H2 and there should be a strain to pull the submerged anticyclone toward deep waters. On the other hand, the subsurface anticyclone should possess an initial impetus to move to shallower waters in order to conserve potential vorticity. The consequent strain across isobaths should enhance fission of submerged anticyclones preferably in cross-isobath directions.

Outcomes of the slope-enhanced fission vary. End configurations frequently seen in the foregoing numerical experiments

are illustrated in Figs. 16b,c,d ⊙. For strong fission, three submerged anticyclones are often produced (Fig. 16b ⊙). If fission is weak, the parent anticyclone can be pulled to deeper waters by the intensifying cyclone C1 (Fig. 16c ⊙), or moves to shallower waters to conserve potential vorticity (Fig. 16d ⊙). In experiment 2S (Fig. 11 ⊙, upper panel), the parent is pulled to deeper waters in ways similar to that depicted in Fig. 16c ⊙. In experiment 3S (Fig. 12 ⊙, upper panel), the parent anticyclone moves to shallower waters in ways similar to that depicted in Fig. 16d ⊙. Top cyclones dissipate in time as a result of ice-exerted friction, leaving submerged anticyclones in stable existence thereafter.

Several other limits not included here are briefly discussed below. If the bottom slope is shifted downward to much greater depths, topographic enhancement of fission disappears. In this limit the flat-bottom and sloping-bottom solutions become visually indistinguishable. If the upper-ocean stratification is reduced, all vortices become stronger under the same brine forcing because downward convection is enhanced. If an oversized brine source much larger than a Rossby radius is used, fission occurs only around the rim and is therefore much weaker. For a very strong brine source (F_0) or a long pulse (T), deep convection would occur, and the dynamic regime is entirely different. In the event of deep convection, the top cyclone would be too deep and too strong to be annihilated by the ice-exerted friction. Typical continental slopes around the rim of the deep Arctic basin are often steeper than the bottom slope used herein. Thus, our model setting is more applicable to the shallow reaches of continental slopes. Nevertheless, it seems reasonable to expect similar physical processes over a steeper slope. We have refrained from approaching the steep-slope limit to avoid truncation errors associated with a σ-coordinate formulation over steep slopes.

Summarizing, a shallow and strong brine source or a sudden placement of a strong salty heton under sea ice generally increases the number of submerged anticyclones. A bottom slope enhances the fission; subsurface vortices after fission tend to align in cross-isobath directions. In comparison, the increase of submerged cyclones under a freshening source is much less likely. The foregoing conclusions hold whether a uniform current is imposed or not. At the present time, it is not known how frequently the density forcing can accumulate to considerable strength in the Arctic Ocean, If this occurs frequently, then the slope-enhanced fission offers an additional mechanism helping explain the ubiquity of subsurface anticyclones under the Arctic sea ice.

Acknowledgments

REFERENCES

Blumberg, A. F., and G. L. Mellor, 1987: A description of a three-dimensional coastal ocean circulation model. *Three-Dimensional Coastal Ocean Models,* N. S. Heaps, Ed., Amer. Geophys. Union, 1–16.

Carsey, F. D., and A. T. Roach, 1994: Oceanic convection in the Greenland Sea Odden region as interpreted in satellite data. *The Polar Oceans and Their Role in Shaping the Global Environment, Geophys. Monogr.* No. 85, Amer. Geophys. Union, 211–222.

Chao, S.-Y., and P.-T. Shaw, 1996: Initialization, asymmetry and spindown of Arctic eddies. *J. Phys. Oceanogr.,* **26,** 2076–2092. Find this article online

—— ,and —— ,1998: Eddy maintenance and attrition in a vertically sheared current under Arctic ice. *J. Phys. Oceanogr.,* **28,** 2427–2443. Find this article online

—— ,and —— ,1999a: Close interactions between two pairs of heton-like vortices under sea ice. *J. Geophys. Res.,* **104,** 23 591–23 605.

—— ,and —— ,1999b: Fission of heton-like vortices under sea ice. *J. Oceanogr.,* **55,** 65–78.

Forsythe, G. E., and C. B. Moler, 1967: *Computer Solution of Linear Algebraic Systems.* Prentice-Hall, 148 pp.

Haney, R. L., 1991: On the pressure gradient force over steep topography in sigma coordinate ocean models. *J. Phys. Oceanogr.,* **21,** 610–619. Find this article online

Hibler, W. D., III, 1979: A dynamic thermodynamic sea ice model. *J. Phys. Oceanogr.,* **9,** 815–846. Find this article online

Hogg, N. G., and H. M. Stommel, 1985: The heton: An elementary interaction between discrete baroclinic geostrophic vortices and its implications concerning eddy heat-flow. *Proc. Roy. Soc. London,* **A397,** 1–20.

Kämpf, J., and J. O. Backhaus, 1998: Shallow, brine-driven free convection in polar oceans: Nonhydrostatic numerical process studies. *J.*

Geophys. Res., 103, 5577–5593.

Manley, T. O., and K. Hunkins, 1985: Mesoscale eddies of the Arctic Ocean. *J. Geophys. Res., 90,* 4911–4930.

Mellor, G. L., and T. Yamada, 1974: A hierarchy of turbulence closure models for planetary boundary layers. *J. Atmos. Sci., 31,* 1791–1806. Find this article online

Nof, D., 1991: Fission of single and multiple eddies. *J. Phys. Oceanogr., 21,* 40–52. Find this article online

Pease, C. H., S. A. Salo, and J. E. Overland, 1983: Drag measurements for first-year sea ice over a shallow sea. *J. Geophys. Res., 88,* 2853–2862.

Rossby, C.-G., 1938: On the mutual adjustment of pressure and velocity distributions in certain simple current systems. *J. Mar. Res., 1,* 239–263.

Saunders, P. M., 1973: The instability of a baroclinic vortex. *J. Phys. Oceanogr., 3,* 61–65. Find this article online

Smith, D. C., and J. H. Morison, 1993: A numerical study of haline convection beneath leads in sea ice. *J. Geophys. Res., 98,* 10 069–10 083.
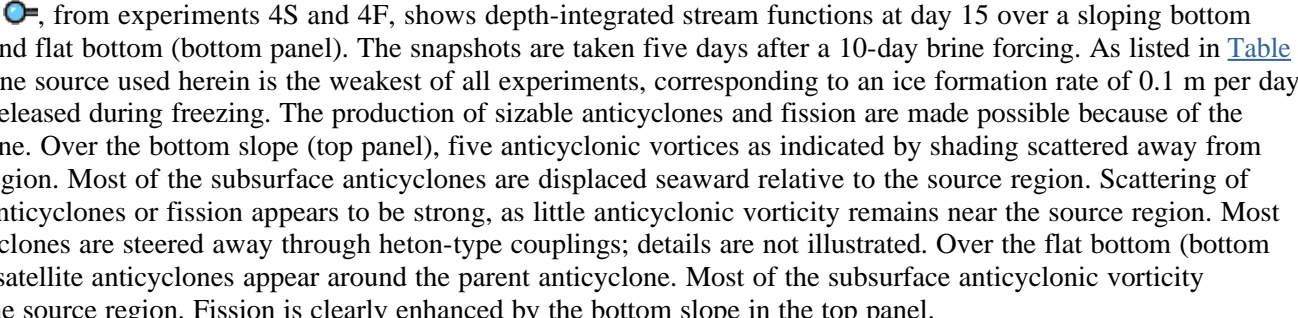
——, R. D. Muench, and C. H. Pease, 1990: Polynyas and leads: An overview of physical processes and environment. *J. Geophys. Res., 95,* 9461–9479.

APPENDIX A

5. A Weak Brine Source in a Weak Halocline

Brine release rates used in the main text are considerably stronger than what a realistic freezing event in a timescale of 10 days can provide. When asked by reviewers to demonstrate slope-enhanced fission produced by a more realistic freezing event in a time scale of 10 days, experiments 4S and 4F were used to explore this limit.

In this limit, the physical setting must not be too far away from land, so that the outbreak of cold air can be dry enough to provoke latent heat loss from open water and seawater freezing. The water depth cannot be substantially shallower than the model basin used in the main text; the downward convection will be otherwise too shallow to produce sizable subsurface anticyclones and fission. Most importantly, the halocline must be sufficiently weak to allow for vigorous downward convection. Few places in the Beaufort Sea fit the description because of the strong halocline there. On the Scandinavia side of the Arctic Ocean, quite a few shelf regions fit the description. The required conditions also can be met in many places in the Antarctic Ocean; the Western Ross Sea is a good example.

Figure A1, from experiments 4S and 4F, shows depth-integrated stream functions at day 15 over a sloping bottom (top panel) and flat bottom (bottom panel). The snapshots are taken five days after a 10-day brine forcing. As listed in Table 1, the brine source used herein is the weakest of all experiments, corresponding to an ice formation rate of 0.1 m per day if all salt is released during freezing. The production of sizable anticyclones and fission are made possible because of the weak halocline. Over the bottom slope (top panel), five anticyclonic vortices as indicated by shading scattered away from the source region. Most of the subsurface anticyclones are displaced seaward relative to the source region. Scattering of subsurface anticyclones or fission appears to be strong, as little anticyclonic vorticity remains near the source region. Most of the anticyclones are steered away through heton-type couplings; details are not illustrated. Over the flat bottom (bottom panel), four satellite anticyclones appear around the parent anticyclone. Most of the subsurface anticyclonic vorticity remains in the source region. Fission is clearly enhanced by the bottom slope in the top panel.

It should be emphasized, however, that rotation speeds of these submerged anticyclones are quite weak, ranging only up to about ~ 2–3 cm s^{-1}. While slope-enhanced fission is possible under a weak source, the resulting subsurface anticyclones are much weaker than the typical energetic anticyclones observed in the Beaufort Sea.

APPENDIX B

6. The Ice Layer

The sea ice model consists of two continuity equations for ice concentration (A) and thickness (h), and two momentum equations for ice drifts (u and υ). These equations are identical to Hibler (1979); details will not be given below. Since the present model domain is much smaller with fine horizontal grid spacing, some parameters are adjusted. Referring to Hibler's Table 1, we have $P* = 4000$ N m^{-1} and $\zeta_{min} = 2 \times 10^7$ kg s^{-1}. Since the ice pressure builds up as A increases, the ice layer produces considerable compressive strength against convergence if A exceeds about 0.8. In this application the initial ice concentration is 0.7; the ice layer behaves more like a highly viscous fluid whether converging or diverging. A modest Laplacian diffusion is added to the continuity equations for ice thickness and concentration with a diffusion coefficient of 200 m^2 s^{-1}.

The time stepping for governing equations is done by a leapfrog scheme with occasional smoothing. The time step is 30 min for the ice layer. Frictional forces due to internal ice stress are rather large. In consequence, all terms related to friction must be treated implicitly, forming large matrices to be inverted. In Hibler (1979), matrix inversions are done by an iterative relaxation scheme. Here, matrices are inverted directly using the standard technique of Gaussian elimination by "LU decomposition" (Forsythe and Moler 1967).

Tables

Table 1. List of experiments. Without mean flow (U_0), experiments are conducted in pairs. Sloping and flat bottom experiments are denoted by "S" and "F," respectively. Eastward and westward mean currents of 5 cm s^{-1} are denoted by "E" and "W," respectively. With mean flow, both eastward and westward currents are imposed over the bottom slope, while only eastward flow is imposed over the flat bottom. The volume average of salinity production rate over a cylindrical source volume of height z_1(=50 m) and radius r_0(=6 km) is denoted by $\langle F \rangle$

| Expt	F_0 (psu day^{-1})	T (days)	h_1 (m)	h_2 (m)	h_b (m)	$\langle F \rangle$ (psu day^{-1})	ΔS (psu)	U_0 (cm s^{-1})
1S	1.05	5	200	500	—	0.59	4.5	0
1F	1.05	5	—	—	350	0.59	4.5	0
2S	0.5	10	200	500	—	0.29	4.5	0
2F	0.5	10	—	—	350	0.29	4.5	0
3S	0.25	10	200	500	—	0.15	4.5	0
3F	0.25	10	—	—	350	0.15	4.5	0
4S	0.125	10	200	500	—	0.075	0.5	0
4F	0.125	10	—	—	350	0.075	0.5	0
1SE	1.05	5	200	500	—	0.59	4.5	5
1SW	1.05	5	200	500	—	0.59	4.5	−5
1FE	1.05	5	—	—	350	0.59	4.5	5
3SE	0.25	10	200	500	—	0.15	4.5	5
3SW	0.25	10	200	500	—	0.15	4.5	−5
3FE	0.25	10	—	—	350	0.15	4.5	5

Click on thumbnail for full-sized image.

Figures
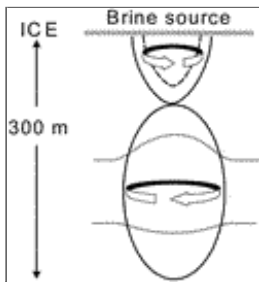
Click on thumbnail for full-sized image.

Fig. 1. A schematic sectional view showing how a brine source generates a pair of vertically stacked eddies. The dashed contour beneath the ice layer indicates the region of brine forcing. Arrows show the sense of rotation, and dotted contours indicate isohalines
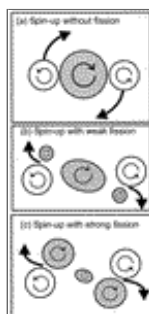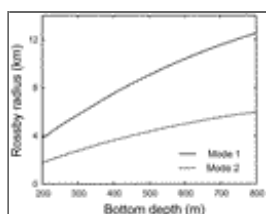

Click on thumbnail for full-sized image.

Fig. 2. Schematic illustrations of fission from a pair of baroclinic eddies induced by a brine source over a flat basin. Top cyclones are not shaded, and subsurface anticyclones are shaded. The initial outbreak of top cyclones is weak in (a), modest in (b), and strong in (c). Through heton-type couplings, fission of the submerged anticyclone becomes progressively stronger from (a) to (c)
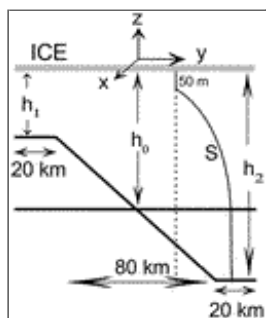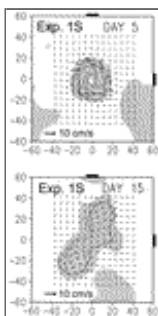

Click on thumbnail for full-sized image.

Fig. 3. A cross-isobath section of the model domain, showing the coordinate system, salinity profile and bottom depth profiles. The water depth either increases in y from h_1 to h_2 in a piecewise-linear fashion or is fixed at h_0

Click on thumbnail for full-sized image.

Fig. 4. The first and second baroclinic Rossby radii as functions of water depth

Click on thumbnail for full-sized image.

Fig. 5. Ice concentrations and drifts at days 5 (top panel) and 15 (bottom panel) for experiment 1S. The contour interval for ice concentrations is 0.1. Shading indicates concentration lower than the initial value of 0.7. The e-folding diameter of the brine source is projected onto x and y axes as bars on top and right of each panel. Similar markings will be made in all plan views hereafter. Water depth increases in the $+y$ direction (pointing toward the top of the page). Coordinates are in km
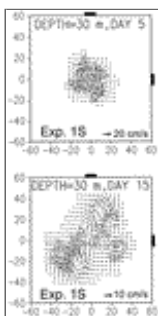
Click on thumbnail for full-sized image.

Fig. 6. Upper ocean flow and salinity fields at 30-m depth for expt 1S at days 5 (top) and 15 (bottom). Shading indicates salinity (psu) higher than 30.52. Coordinates are in km
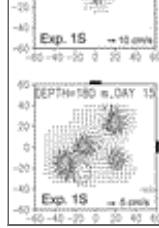
Fig. 7. As in [Fig. 6](#) ⊙▬ except at 180-m depth. Salinity (psu) contour values are 31.7 and 31.8; shading indicates salinity lower than 31.75
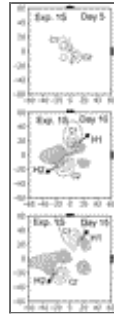
Fig. 8. Vertically integrated stream functions at days 5 (top panel), 10 (middle panel), and 15 (bottom panel) for expt 1S. Nonzero streamlines are contoured at intervals of 4×10^4 m^3 s^{-1}. Shading indicates contour values higher than 2×10^4 m^3 s^{-1} in the top panel, and 4×10^4 m^3 s^{-1} in the lower two panels. Heton-type couplings associated with shallow cyclones C1 and C2 are indicated by H1 and H2, respectively. Coordinates are in km
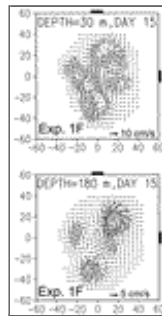
Fig. 9. Flow and salinity fields at day 15 in expt 1F at 30 m (top panel) and 180 m (bottom panel) depths. Shading indicates salinity (psu) higher than 30.53 at 30-m depth and lower than 31.75 at 180-m depth. Salinity contours in the lower panel are 31.7 and 31.8. Coordinates are in km
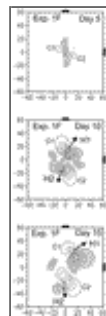
Fig. 10. As in [Fig. 8](#) ⊙▬ except for experiment 1F
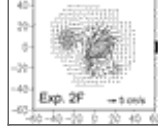
Fig. 11. Flow and salinity fields at day 15 and 180-m depth from expts 2S (upper panel) and 2F (lower panel). Shading indicates salinity (psu) lower than 31.75 in both panels. Salinity values are contoured at 31.7 and 31.8. Coordinates are in km
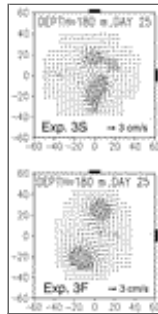
Fig. 12. As in Fig. 11 except for experiments 3S and 3F at day 25. Shading indicates salinity lower than 31.755 psu
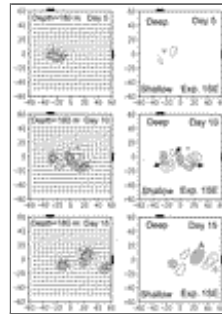
Fig. 13. Flow and density fields at 180-m depth (left panels) and perturbation streamlines (right panels) for expt 1SE at days 5, 10, and 15. Ambient eastward flow is 5 cm s^{-1} but weakened somewhat by bottom friction over the shallow shelf to the south. Anomalies of vertically integrated streamlines are obtained after removing the zonal average. Arrows in right panels indicate copropagation tendency due to heton-type couplings. Shading scales and contour values are identical to Fig. 11 for flow and salinity, and to Fig. 8 for streamlines. Bars on top and right of each panel indicate the stationary brine location. Coordinates are in km
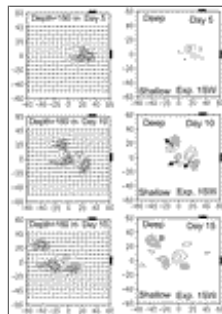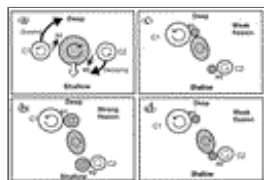
Fig. 14. As in Fig. 13 except for expt 1SW, in which a westward mean flow of 5 cm s^{-1} is imposed over the bottom slope

Fig. 15. As in Fig. 13 ⊙= except for expt 1FE, in which an eastward flow of 5 cm s^{-1} is imposed over the flat-bottomed basin

Fig. 16. Schematic illustrations of fission from a pair of baroclinic eddies induced by a brine source over a sloping bottom. Shallow cyclones and submerged anticyclones are unshaded and shaded, respectively. Here, C1 and C2 are two cyclones breaking away initially; H1 and H2 are the hetons formed. See text
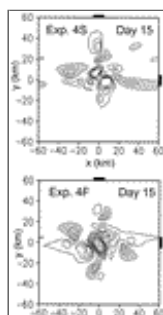
Fig. A1. Depth-integrated stream functions at day 15 from expts 4S (top panel) and 4F (bottom panel). Nonzero streamlines are contoured at intervals of 1×10^4 m^3 s^{-1}. Shading indicates anticyclonic vorticity. Water depth increases in y in the top panel

Corresponding author address: Dr. Shenn-Yu Chao, Horn Point Environmental Laboratory, University of Maryland System, Cambridge, MD 21613-0775.

E-mail: chao@hpl.umces.edu

top ▲